Journal of Cerebral Blood Flow & Metabolism (2015) 35, 1411–1415

www.jcbfm.com

BRIEF COMMUNICATION

Arteriole dilation to synaptic activation that is sub-threshold to astrocyte endfoot Ca^{2+} transients

Ádám Institoris[1,2], David George Rosenegger[1] and Grant Robert Gordon[1]

Ca^{2+}-dependent pathways in neurons and astrocyte endfeet initiate changes in arteriole diameter to regulate local brain blood flow. Whether there exists a threshold of synaptic activity in which arteriole diameter is controlled independent of astrocyte endfeet Ca^{2+} remains unclear. We used two-photon fluorescence microscopy to examine synaptically evoked synthetic or genetic Ca^{2+} indicator signals around penetrating arterioles in acute slices of the rat neocortex. We discovered a threshold below which vasodilation occurred in the absence of endfeet Ca^{2+} signals but with consistent neuronal Ca^{2+} transients, suggesting endfoot Ca^{2+} is not necessary for activity-dependent vasodilation under subtle degrees of brain activation.

Journal of Cerebral Blood Flow & Metabolism (2015) **35,** 1411–1415; doi:10.1038/jcbfm.2015.141; published online 1 July 2015

Keywords: calcium imaging; cerebral blood flow; functional hyperemia; GCaMP; neurovascular coupling

INTRODUCTION

Neurovascular coupling provides moment-to-moment regulation of brain blood flow by controlling arteriole diameter when synaptic activity increases via activation of neuronal and astrocytic processes.[1] Diameter changes are initiated by Ca^{2+} signaling in either astrocytic endfeet,[2,3] which wrap cerebral arterioles, or neuronal elements.[1,4] Whether astrocyte and neuron control over arteriole diameter is inextricably tied together or whether this dual cell-type control can be functionally separated during specific intensities of afferent activity remains unclear.

Early brain slice studies showed that when the tissue was robustly stimulated electrically, astrocyte Ca^{2+} transients in somata and endfeet were evoked and preceded vascular responses.[5,6] Uncaging Ca^{2+} in astrocytes clearly defined the endfoot as the point of communication to the arteriole.[2] Subsequent *in vivo* studies observed astrocyte endfoot Ca^{2+} that preceded vasodilation after functional stimulation using bulk-loaded acetoxymethyl ester (AM) dyes,[7–9] while others that systematically tested the cellular source of Ca^{2+} failed to observe the endfoot signals expected to participate in vasodilation.[10,11]

We used two-photon fluorescent imaging in acute brain slices of the rat sensory-motor cortex to control the location and intensity (voltage) of electrical afferent stimulation while recording Ca^{2+} transients in astrocytes and neurons using synthetic and genetically encoded indicators. We tested the hypothesis that afferent fiber activation below a particular threshold initiates vasodilation with consistent neuronal Ca^{2+} signals but in the absence of astrocyte endfeet Ca^{2+} transients.

MATERIALS AND METHODS

The Animal Care and Use committee of the University of Calgary (protocol M11002) approved all procedures abiding by Canadian standards for animal research and complying with ARRIVE guidelines. Male Sprague Dawley rats (P21-50, Charles River, Wilmington, MA, USA) received an intravenous injection of fluorescein isothiocyanate–dextran (FITC-dextran) (Sigma-Aldrich, St. Louis, MO, USA, 2,000 KDa; 15 mg in 0.4 ml lactated ringers) or rhodamine-B isothiocyanate–dextran (Rhod-dextran) (Sigma-Aldrich, 70 KDa; 12 mg in 0.3 ml) to label the vasculature. Acute 400-μm thick coronal slices of the sensory-motor cortex were cut with a vibratome (Leica VT1200S, Wetzlar, Germany) and incubated in artificial cerebrospinal fluid (ACSF) saturated with 95% O_2/5% CO_2 for 45 minutes at 34°C. ACSF contained (in mmol/L): NaCl (126), KCl (2.5), $NaHCO_3$ (25), $CaCl_2$ (1.5), $MgCl_2$ (1.2), NaH_2PO_4 (1.25), and glucose (10). Imaging was performed at 22°C and slices were superfused at ~2 ml/min. The arteriole preconstrictor U46619 (Cayman Chemical, Ann Arbor, MI, USA) (100 nmol/L) was added to the bath for all experiments.[4,6] Imaging used a custom made two-photon microscope fitted with a ×40 W/1.00 NA Zeiss objective lens and a Chameleon Ultra Ti:Sapph laser (Coherent, Santa Clara, CA, USA). Time series used a field size of 200 to 290 μm^2 at 0.98 Hz (512 pixels^2) or a field size of 26 to 32 μm^2 at 31.25 Hz (128 pixels^2). A single focal plane captured the middle, top, or bottom of an arteriole lumen (diameter: ~10 to 50 μm; cortical layer: 1 to 3; imaging depth: 50 to 100 μm).

Rhod-2/AM (Biotium Inc.) (15 μmol/L) was dissolved in ACSF containing 0.2% dimethyl sulfoxide, 0.006% pluronic acid (Life Technologies, Carlsbad, CA, USA), and 0.0002% Cremphor EL (Sigma-Aldrich) and incubated for 45 minutes at 34°C after the 45 minutes recovery from slicing. Oregon Green 488 BAPTA-1/AM (OGB-1/AM, Life Technologies) was dissolved in ACSF to 500 μmol/L containing 7.5% dimethyl sulfoxide and 1.25% pluronic acid, and was microinjected[10] into the slice adjacent to an arteriole under study. Imaging started ~1 hour after injection. Astrocytes were identified by the presence of endfeet apposed to the vasculature.

[1]Hotchkiss Brain Institute, Department of Physiology and Pharmacology, Cumming School of Medicine, University of Calgary, Calgary, Alberta, Canada and [2]Department of Physiology, Faculty of Medicine, University of Szeged, Szeged, Hungary. Correspondence: Dr GR Gordon, Department of Physiology and Pharmacology, Hotchkiss Brain Institute, Cumming Faculty of Medicine, University of Calgary, 3330 Hospital Dr NW, Room 1B40A, Building HRIC, Calgary, AB T2N 4N1, Canada.
E-mail: grjgordo@gmail.com
The Canadian Institutes of Health Research and the Heart and Stroke Foundation of Canada supported this study. Canada Research Chairs and the Heart and Stroke Foundation Alberta supported GRG. Alberta Innovates Health Solutions supported DGR.
Received 21 January 2015; revised 15 May 2015; accepted 18 May 2015; published online 1 July 2015

For cyto-GCaMP3 or lck-GCaMP6f, P21-22 rats received intracortical delivery of an adeno-associated virus (AAV2/5-gfaABC1D-cyto-GCaMP3 or AAV2/5-gfaABC1D-lck-GCaMP6f, Penn Vector Core, Philadelphia, PA, USA), two to four weeks before the experiment. A volume of 207 nL (9.0×10^9 particles) was delivered via a Nanoject II (Drummond Scientific, Broomall, PA, USA) under 2% isoflurane anesthesia. Ca^{2+} signals from neurons, neuropil, astrocyte somata, and endfeet were analyzed using ImageJ (National Institutes of Health, Bethesda, MD, USA) and Prism software (GraphPad, La Jolla, CA, USA) as $\Delta F/F = ((F_1 - F_0)/F_0)x100$. Arteriole diameter measurements represent the area change of the vascular lumen. A diameter change or a Ca^{2+} signal was defined as a value >3 s.d. from baseline variation. All endfeet in the image were examined for possible localized or widespread Ca^{2+} signals between stimulation onset and the onset of vasodilation. If none occurred, the same endfoot/endfeet region of interest that showed a supra-threshold Ca^{2+} signal was used for the sub-threshold data set.

Electrical stimulation used a Grass S88X stimulator (Grass Technologies, Middleton, WI, USA), voltage-isolation unit, and a concentric bipolar electrode (FHC, Bowdoin, ME, USA) positioned ~300 μm lateral from the arteriole. As our question pertained to the fidelity of endfoot Ca^{2+} to vasodilation, if low-intensity afferent stimulation produced vasoconstriction the experiment was not further pursued. Sub-threshold intensity refers to the highest stimulation voltage where only neural Ca^{2+} and vascular diameter changes were observed and supra-threshold intensity indicates the lowest stimulation voltage where neuronal+astrocyte endfeet Ca^{2+} signals and vascular diameter changes were detected. Sub to supra differed by 0.1 to 0.2 V in a given experiment. Voltage range was 0.75 to 2 V across all experiments.

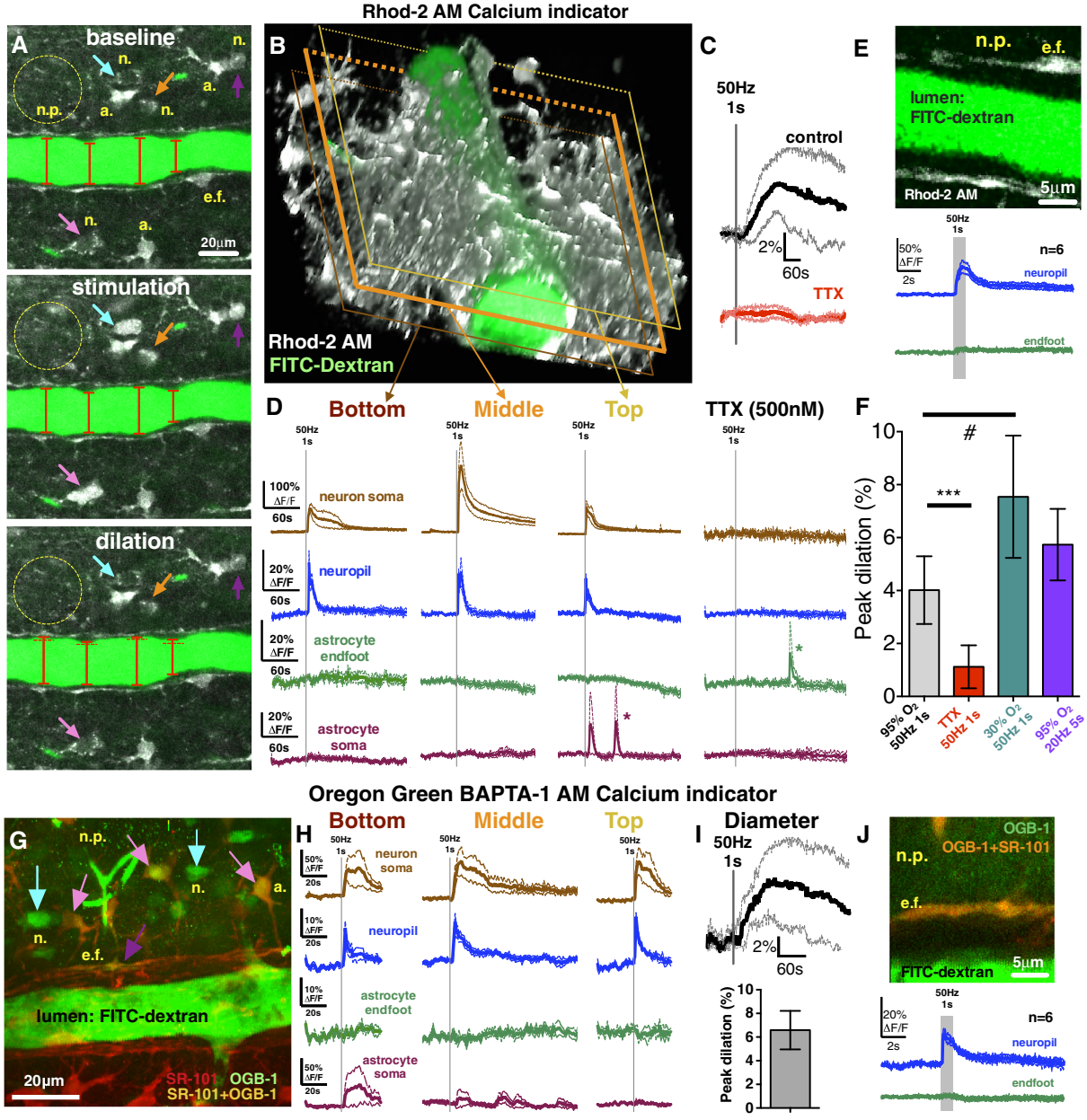

RESULTS

To test the hypothesis that afferent fiber activation initiates vasodilation independent of astrocyte endfeet Ca^{2+} transients when below a particular threshold, we imaged either the large dynamic range Ca^{2+} indicator Rhod-2/AM or the high-affinity Ca^{2+} indicator OGB-1/AM and steadily increased the voltage of brief (1 second), high frequency (50 Hz) electrical stimulation by 0.1 V per trial. Ramping stimulation eventually triggered neuropil ($\Delta F/F_{Rhod\text{-}2} = 21\% \pm 7\%$; $\Delta F/F_{OGB\text{-}1} = 14\% \pm 2\%$) and neuron somata Ca^{2+} signals ($\Delta F/F_{Rhod\text{-}2} = 252\% \pm 87\%$; $\Delta F/F_{OGB\text{-}1} = 71\% \pm 26\%$) that were time locked to the stimulation and preceded the onset of vasodilation (Rhod-2/AM experiments: $4.0\% \pm 0.5\%$, $n = 6$; Figures 1A–1D; OGB-1/AM experiments: $7.8\% \pm 1.5\%$, $n = 6$; Figures 1G–1I) by 39 ± 25 seconds (mean ± s.d.). Notably, the neuropil Ca^{2+} signal spread uniformly across the entire imaging field and encompassed the arteriole. These events were triggered at a particular threshold of minimal afferent stimulation with neither the appearance of astrocyte somata ($\Delta F/F_{Rhod\text{-}2} = 3\% \pm 2\%$; $\Delta F/F_{OGB\text{-}1} = 14\% \pm 15\%$) nor endfeet ($\Delta F/F_{Rhod\text{-}2} = 1\% \pm 1\%$; $\Delta F/F_{OGB\text{-}1} = 2\% \pm 1\%$) Ca^{2+} transients (Rhod-2 Figure 1D; OGB-1 Figure 1H). We tested the possibility that when imaging a single focal plane centered through the arteriole lumen, we missed endfoot Ca^{2+} transients that occurred above or below the plane examined. By using the same stimulation voltage that evoked dilation without endfeet Ca^{2+} transients, we repeated the trial at two additional image planes. Neither a more superficial (top: $\Delta F/F_{Rhod\text{-}2} = 2\% \pm 1\%$; $\Delta F/F_{OGB\text{-}1} = 1\% \pm 1\%$) nor a deeper (bottom: $\Delta F/F_{Rhod\text{-}2} = 3\% \pm 2\%$; $\Delta F/F_{OGB\text{-}1} = 3\% \pm 1\%$) image plane of the arteriole revealed endfeet Ca^{2+} transients, despite clear neuropil (top: $\Delta F/F_{Rhod\text{-}2} = 19\% \pm 2\%$; $\Delta F/F_{OGB\text{-}1} = 18\% \pm 1\%$; bottom: $\Delta F/F_{Rhod\text{-}2} = 26\% \pm 6\%$; $\Delta F/F_{OGB\text{-}1} = 14\% \pm 2\%$) and neuron somata (top: $\Delta F/F_{Rhod\text{-}2} = 105\% \pm 23\%$; $\Delta F/F_{OGB\text{-}1} = 76\% \pm 26\%$; bottom: $\Delta F/F_{Rhod\text{-}2} = 86\% \pm 14\%$; $\Delta F/F_{OGB\text{-}1} = 53\% \pm 33\%$) Ca^{2+} transients (Rhod-2 Figure 1D; OGB-1 Figure 1H). Blocking voltage-gated sodium channels with tetrodotoxin (TTX, 500 nmol/L) eliminated the change in arteriole diameter ($0.3\% \pm 0.4\%$, Figure 1C; peak: $1.1\% \pm 0.4\%$, Figure 1F), as well as both the neuropil ($\Delta F/F_{Rhod\text{-}2} = 2\% \pm 1\%$) and neuronal somata ($\Delta F/F_{Rhod\text{-}2} = 2\% \pm 1\%$) Ca^{2+} signals ($n = 6$, Figures 1C and 1D). Next, we investigated the possibility that imaging at a temporal resolution of 0.98 Hz (frame acquisition) was too slow to detect a fast astrocyte Ca^{2+} transient.[9] We imaged neuropil and endfeet apposed to the region of peak vasodilation at 31.25 Hz (32 ms per frame). The neuropil Ca^{2+} signal was again reliably evoked ($\Delta F/F_{Rhod\text{-}2} = 43\% \pm 10\%$; $\Delta F/F_{OGB\text{-}1} = 16\% \pm 2\%$) within 32 to 64 ms from stimulation onset, but we did not detect endfoot Ca^{2+} transients ($n = 6$, $\Delta F/F_{Rhod\text{-}2} = 7\% \pm 2\%$; $\Delta F/F_{OGB\text{-}1} = 5\% \pm 3\%$; Rhod-2, Figure 1E; OGB-1, Figure 1J). We then tested if a different pattern of afferent fiber activity produced analogous results. Stimulating electrically at 20 Hz for 5 seconds still failed to trigger reliable astrocyte somata ($\Delta F/F_{Rhod\text{-}2} = 3\% \pm 2\%$) or endfeet Ca^{2+} transients ($\Delta F/F_{Rhod\text{-}2} = 0\% \pm 1\%$) that preceded vasodilation ($5.7\% \pm 0.6\%$; $n = 6$, Figure 1F). Collectively, these data show that there exists a level of afferent fiber activation that causes vasodilation in the absence of Ca^{2+} signals from astrocyte somata and endfeet (Supplementary Video S1).

Standard slice conditions provide elevated oxygen, which attenuates vasodilation because of the recruitment of cell pathways that promote constriction.[3] We confirmed that a lower ambient O_2 concentration (bubbling ACSF with 30% O_2) evoked larger vasodilation ($7.5\% \pm 0.9\%$, $n = 7$; Figure 1F) compared with 95% O_2 in response to 50 Hz 1-second stimulation ($P < 0.05$). This magnitude of diameter change translates into an ~34% blood flow increase. Furthermore, oxygen may affect the threshold of astrocyte activation because of an influence on extracellular adenosine and transmitter release probability.[3] However, low O_2 vasodilations were similarly associated with the clear appearance of neuropil Ca^{2+} ($\Delta F/F_{Rhod\text{-}2} = 24\% \pm 4\%$) and lack of endfoot activity ($\Delta F/F_{Rhod\text{-}2} = 4\% \pm 1\%$).

Next, we tested if the stimulation voltages that were sub-threshold for endfeet Ca^{2+} became supra-threshold at higher voltages. Indeed, an increment of 0.1 to 0.2 V was met with more consistent Ca^{2+} transients in astrocyte somata ($\Delta F/F_{Rhod\text{-}2} = 117\% \pm 44\%$; $\Delta F/F_{OGB\text{-}1} = 64\% \pm 10\%$) and the appearance of endfeet signals ($\Delta F/F_{Rhod\text{-}2} = 42\% \pm 19\%$, Figure 2A; $\Delta F/F_{OGB\text{-}1} = 16\% \pm 6\%$; Supplementary Figure S1). Using fast imaging, we found that supra-threshold stimulation evoked both neuropil ($\Delta F/F_{OGB\text{-}1} = 33\% \pm 9\%$; $latency_{OGB\text{-}1}$: < 32 ms, $latency_{Rhod\text{-}2}$: 32 to 64 ms) and endfoot signal ($\Delta F/F_{OGB\text{-}1} = 18\% \pm 10\%$; latency: 3.18 ± 1.55 seconds; Supplementary Figure S1). These astrocyte Ca^{2+} transients preceded vasodilation that was of similar magnitude to respective sub-threshold dilation (Rhod-2 experiments: sub = $4.5\% \pm 0.8\%$ versus supra = $5.0\% \pm 0.4\%$, $n = 7$; Figure 2B; OGB-1 experiments: sub = $7.8\% \pm 1.5\%$ versus supra = $7.6\% \pm 2.6\%$, Figure 1I; Supplementary Figure S1). A subset of supra-threshold stimulations was repeated in the presence of TTX, which prevented all Ca^{2+} signals (data not shown) and diameter changes ($0.9\% \pm 1\%$, $n = 5$). These data show that only after a particular threshold of afferent activity is reached are endfoot Ca^{2+} transients observed preceding vasodilation.

To test whether the globally distributed neuropil Ca^{2+} signal and the putative endfoot Ca^{2+} signals were of astrocytic origin, we used genetically encoded Ca^{2+} indicators via AAV2/5 to enable

Figure 1. Low-intensity afferent neural activity caused vasodilation in the absence of astrocyte Ca^{2+} transients. (**A**) Penetrating arteriole and surrounding brain cells during baseline, electrical stimulation (50 Hz for 1 second), and peak of stimulus-evoked dilation (a., astrocyte soma; e.f., endfoot; n., neuron soma; n.p., neuropil). Vascular lumen loaded with FITC–dextran (green); neurons and astrocytes bulk loaded with the synthetic Ca^{2+} indicator Rhod-2/AM (gray). Colored arrows point to different neurons activated by the stimulation. Astrocytes showed no Ca^{2+} signals. (**B**) Three-dimensional reconstructed z-stack of the same penetrating arteriole. (**C**) Stimulation-induced arteriolar dilation (averaged traces) in the middle imaging plane. (**D**) Low-voltage stimulation triggered Ca^{2+} elevation in the neuropil and neuron somata but not in astrocyte endfeet and somata. Endfoot Ca^{2+} transients were also absent at more superficial (top) or deeper (bottom) imaging depths. Asterisks denote putative spontaneous Ca^{2+} transients. Tetrodotoxin (TTX) completely blocked neuronal Ca^{2+} signals (**D**, right) and dilation (**C**). (**E**) 31.25 Hz scanning of single endfeet failed to capture stimulus-induced fast Ca^{2+} signals. However, a fast neuropil Ca^{2+} signal was consistently evoked by low-voltage 50 Hz stimulation for 1 second. (**F**) Summary peak dilation values to low-intensity stimulation in different O_2 tensions (95% and 30%), stimulation paradigm (50 Hz, 1 second and 20 Hz, 5 seconds), and after TTX treatment. Paired *t*-test showed a significant difference (***$P < 0.001$) between control and TTX-treated dilations. Unpaired *t*-test showed a significant difference ($^{\#}P < 0.05$) between dilations in 95% versus 30% O_2 conditions. (**G**) A maximum intensity z-projection of a penetrating arteriole loaded with FITC–dextran and adjacent brain tissue bulk loaded with the structural dye SR-101 (red) to label astrocytes and microinjected with the synthetic Ca^{2+} indicator Oregon Green 488 BAPTA-1 AM (OGB-1/AM) to load neurons (n., blue arrows), astrocyte somata (a., pink arrows), and endfeet (e.f., purple arrow). (**H**) Low-voltage stimulation evoked neuropil and neuron soma Ca^{2+} transients in all the three imaging depths with the occasional appearance of astrocyte soma Ca^{2+} elevations but without endfoot Ca^{2+} events. (**I**) Stimulation-induced arteriolar dilation (upper graph: averaged trace; bottom graph: peak dilation) in the middle imaging plane of SR-101 and OGB-1/AM-loaded brain slices. (**J**) Using 31.25 Hz scanning, Ca^{2+} transients were not detected in endfeet loaded with OGB-1/AM and SR-101 (green trace) in response to low-intensity stimulation, whereas neuropil Ca^{2+} transients were reliably detected (blue trace). Traces represent averaged summary data showing the mean (thick solid line) with accompanying s.e.m. (surrounding thin dotted lines).

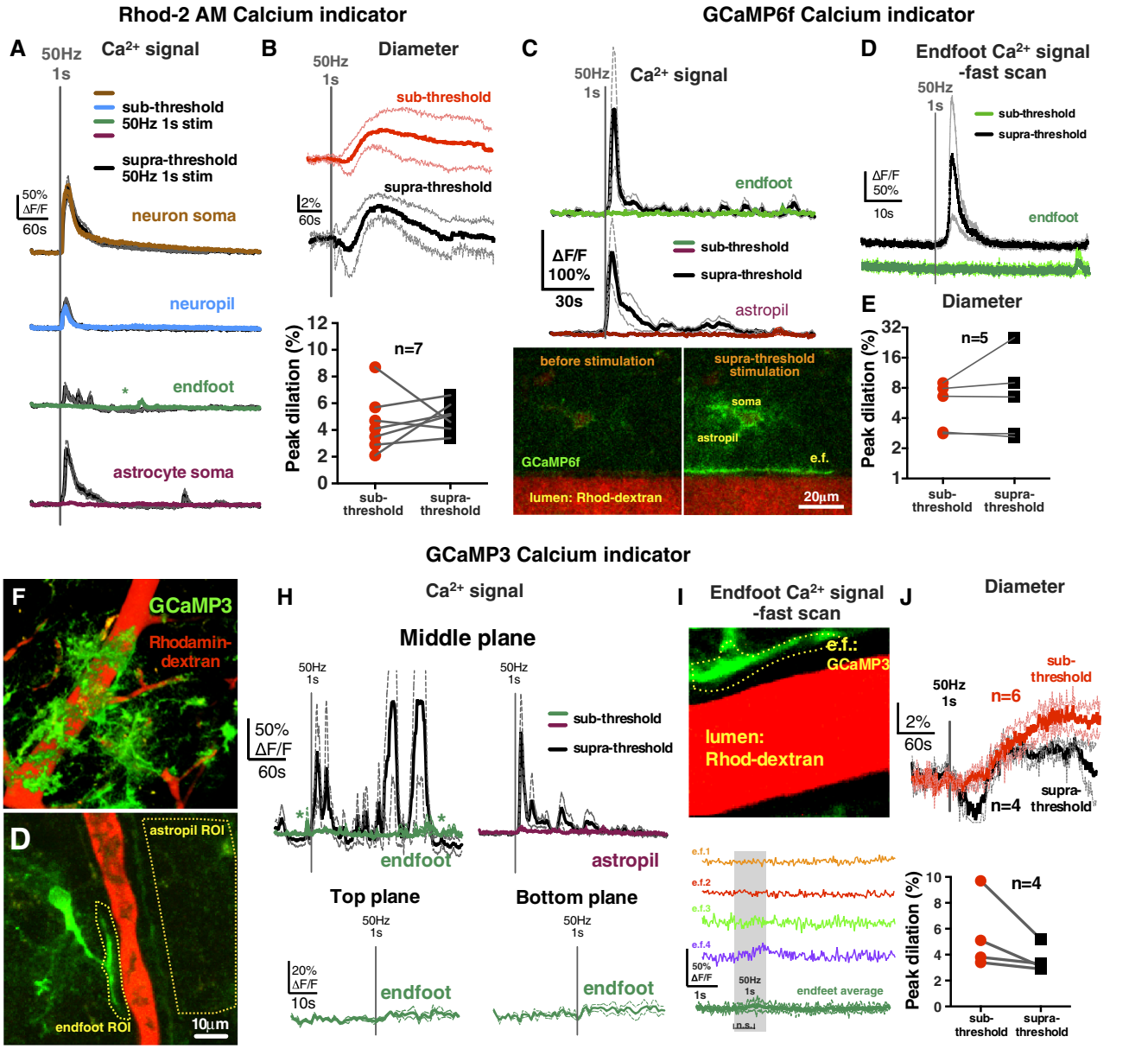

Figure 2. High-intensity afferent neural activity additionally recruited astrocyte Ca^{2+} signals that preceded vasodilation detected with a synthetic Ca^{2+} indicator (Rhod-2/AM) or with either of two astrocyte-specific genetic Ca^{2+} indicators (cyto-GCaMP3 and lck-GCaMP6f). (**A**) Brief (1 second), high frequency (50 Hz) electrical stimulation triggered astrocyte somata, and endfeet Ca^{2+} transients only at higher voltages (supra-threshold) whereas lower voltages evoked Ca^{2+} signals only in neuron somata and neuropil (sub-threshold) detected with Rhod-2/AM. Asterisk denote putative spontaneous Ca^{2+} transients. (**B**) Averaged stimulus-evoked arteriolar dilation to sub-threshold (red) and supra-threshold (black) voltages, and the summary of paired peak dilations. Supra-threshold dilation was not different from sub-threshold dilation. (**C**) Upper: Endfoot Ca^{2+} transients were observed with GCaMP6f in endfeet after supra-threshold but not after sub-threshold electrical stimulation. Astrocyte fine processes (termed astropil) close to the arteriole did not exhibit Ca^{2+} transients to sub-threshold stimulation, whereas supra-threshold stimulation caused an astropil signal. Lower: images a GCaMP6f expressing astrocyte and endfoot apposed to an arteriole before (left) and after (right) supra-threshold stimulation showing the elevation in Ca^{2+}. (**D**) Traces of endfoot Ca^{2+} signals to sub-threshold (green) and supra-threshold (black) stimulation imaged at 31.25 Hz. Only supra-threshold stimulation elicited a Ca^{2+} transient. (**E**) Vasodilation peaks to sub-threshold and supra-threshold stimulations in GCaMP6f-labeled brain slices showed no statistical difference. (**F**) Maximum projection image of a penetrating arteriole (red) and surrounding astrocytes expressing GCaMP3 (green). (**G**) Image of a GCaMP3 astrocyte with an endfoot process apposed to an arteriole. Dashed yellow lines outline a region of interest (ROI) used for analysis. (**H**) Endfoot and astropil Ca^{2+} transients were observed with GCaMP3 after supra-threshold but not after sub-threshold electrical stimulation. Asterisks denote putative spontaneous Ca^{2+} signals. In the top and bottom image plane, stimulus-induced endfeet signals were also absent during sub-threshold stimulation. (**I**) Upper: High-magnification image of a single endfoot expressing GCaMP3 apposed to an arteriole (lumen in red). Yellow-dashed ROI for analysis was shown. Lower: colored Ca^{2+} traces of different endfeet from four experiments imaged at 31.25 Hz. Green summary trace shows no difference between baseline and the highest data points 1 second after stimulation (n.s., nonsignificant). (**J**) Averaged stimulus–evoked arteriolar dilation to sub-threshold (red) and supra-threshold (black) voltages, and the summary of paired peak dilations. Supra-threshold dilation was not different from sub-threshold dilation. Averaged traces are presented as the mean (solid thick line) with accompanying s.e.m. (thin dotted lines).

astrocyte-specific Ca^{2+} measurements in the cytosol using a diffusible cyto-GCaMP3, or in plasma membrane microdomains using membrane anchored lck-GCaMP6f, each driven by a truncated glial fibrillary acidic protein promoter.[12] Again, we could elicit vasodilation (GCaMP3 experiments: 6.5% ± 1.1%, $n = 6$, Figure 2J; GCaMP6f experiments: 5.8% ± 1.2%, $n = 5$, Figure 2E) in the absence of endfoot Ca^{2+} transients either at the central imaging plane ($\Delta F/F_{GCaMP3} = 4\% \pm 2\%$, $n = 6$, Figure 2H; $\Delta F/F_{GCaMP6f} = 1\% \pm 2\%$, $n = 5$, Figure 2C), a more superficial plane (top: $\Delta F/F_{GCaMP3} = 5\% \pm 0.1\%$, $n = 3$), or a deeper imaging plane (bottom: $\Delta F/F_{GCaMP3} = 5\% \pm 2\%$, $n = 3$, Figure 2H). The GCaMPs enabled the visualization of the astrocytic component of the neuropil region (termed astropil). We failed to observe evoked Ca^{2+} transients in the astropil in the vicinity of the arteriole ($\Delta F/F_{GCaMP3} = 5\% \pm 3\%$, $n = 6$, Figure 2H; $\Delta F/F_{GCaMP6f} = 0\% \pm 2\%$, Figure 2C), but could detect the signal close to the stimulating electrode. This was unlike the global neuropil signal observed using Rhod-2 or OGB-1, suggesting a neuronal, rather than astrocytic origin. Notably, as we increased stimulation voltage, supra-threshold stimulation generated the spreading activation of the astropil ($\Delta F/F_{GCaMP3} = 125\% \pm 46\%$, Figure 2H; $\Delta F/F_{GCaMP6f} = 139\% \pm 57\%$, Figure 2C) and endfeet ($\Delta F/F_{GCaMP3} = 102\% \pm 57\%$, Figure 2H; $\Delta F/F_{GCaMP6f} = 180\% \pm 97\%$, Figure 2C) as well as caused vasodilation (GCaMP3 = 3.6% ± 0.5%, $n = 4$, Figure 2J; GCaMP6f = 9.2% ± 4.2%, $n = 5$, Figure 2E). When measuring endfeet at 31.25 Hz image acquisition using GCaMPs at sub-threshold stimulation voltages, we did not detect reliable endfoot Ca^{2+} transients ($\Delta F/F_{GCaMP3} = 6\% \pm 5\%$, Figure 2I; $\Delta F/F_{GCaMP6f} = 2\% \pm 5\%$, Figure 2D) but with supra-threshold stimulation we captured endfoot Ca^{2+} elevation ($\Delta F/F_{GCaMP6f} = 156\% \pm 105\%$, $n = 5$, Figure 2D) with a 4.07 ± 0.92 second latency. These data show that a similar vasodilation that is sub-threshold to astrocyte activation occurs when using genetic Ca^{2+} indicators and that the fast neuropil signal is likely of neuronal origin.

DISCUSSION

Our results help clarify conflicting observations on the presence versus absence of endfoot Ca^{2+} transients during functional hyperemia *in vivo*[7,8,10,11,13] by providing evidence of a specific threshold of afferent activity that must be reached to evoke endfoot Ca^{2+} signals.[14] This suggests that neural elements alone can elicit vasodilation below a particular threshold. Our sub-threshold result is coherent with recent *in vivo* publications that largely failed to observe astrocyte activity.[10,11] Other *in vivo* studies that showed endfeet Ca^{2+} signals preceding vasodilation[7,8,9] may have evoked similar supra-threshold afferent activity as that seen in our experiments, or alternatively such signals may have resulted from the infiltration of neuronal Ca^{2+} signals from bulk-loaded AM-conjugated indicators because of quickly degrading z-resolution with imaging depth.[15]

Although brain slice preparations have a number of drawbacks including a lack of blood flow, realistic tone, reduced temperature, etc., these preparations make it possible to control the location, duration, and intensity of axonal stimulation without intervening natural signals that may arise *in vivo*. Though we used the latest detection tools and did not observe Ca^{2+} transients at low voltage, there remains the possibility that a Ca^{2+} event (1) occurred below our threshold for detection or (2) was not captured because of a lack of interpolated capture and analysis.[9] Nevertheless, our data can be compared with the literature until the sensitivity of future tools surpasses what is currently available.

Our data suggest that endfoot Ca^{2+} is regulated separately from the astrocyte soma. However, the contribution of endfeet Ca^{2+} was not obvious, as vasodilation was similar in magnitude and duration in both sub-threshold and supra-threshold conditions. This may be due to 1) a ceiling effect on diameter, 2) the fact that the difference in voltage applied between sub-threshold and supra-threshold was minor, or 3) the recruitment of a competing constriction pathway at supra-threshold stimulation.[2,3] The mechanism for how astrocytes became activated at higher stimulation voltage was likely the result of enhanced glutamate spillover from the synaptic cleft.[13] Future work will need to expand on how this dual cell-type control of the vasculature by neurons and astrocyte is separately regulated.

AUTHOR CONTRIBUTIONS

AI contributed conceptually to the project, performed the majority of experiments and analysis, prepared the figures, and wrote the manuscript. DGR performed some experiments and analysis for the project, contributed conceptually, and helped in editing the manuscript. GRG contributed conceptually to the project, helped in creating the figures, and wrote the manuscript.

DISCLOSURE/CONFLICT OF INTEREST

The authors declare no conflict of interest.

ACKNOWLEDGMENTS

The authors thank Dr Baljit Khakh for sharing AAVs for GCaMP expression in astrocytes.

REFERENCES

1 Attwell D, Buchan AM, Charpak S, Lauritzen M, MacVicar BA, Newman EA. Glial and neuronal control of brain blood flow. *Nature* 2010; **468**: 232–243.
2 Mulligan SJ, MacVicar BA. Calcium transients in astrocyte endfeet cause cerebrovascular constrictions. *Nature* 2004; **431**: 195–199.
3 Gordon GRJ, Choi HB, Rungta RL, Ellis-Davies GCR, MacVicar BA. Brain metabolism dictates the polarity of astrocyte control over arterioles. *Nature* 2008; **456**: 745–749.
4 Cauli B, Tong X-K, Rancillac A, Serluca N, Lambolez B, Rossier J *et al.* Cortical GABA interneurons in neurovascular coupling: relays for subcortical vasoactive pathways. *J Neurosci* 2004; **24**: 8940–8949.
5 Zonta M, Angulo MC, Gobbo S, Rosengarten B, Hossmann KA, Pozzan T *et al.* Neuron-to-astrocyte signaling is central to the dynamic control of brain microcirculation. *Nat Neurosci* 2003; **6**: 43–50.
6 Filosa JA. Calcium dynamics in cortical astrocytes and arterioles during neurovascular coupling. *Circ Res* 2004; **95**: e73–e81.
7 Takano T, Tian GF, Peng W, Lou N, Libionka W, Han X *et al.* Astrocyte-mediated control of cerebral blood flow. *Nat Neurosci* 2006; **9**: 260–267.
8 Winship IR, Plaa N, Murphy TH. Rapid astrocyte calcium signals correlate with neuronal activity and onset of the hemodynamic response in vivo. *J Neurosci* 2007; **27**: 6268–6272.
9 Lind BL, Brazhe AR, Jessen SB, Tan FCC, Lauritzen MJ. Rapid stimulus-evoked astrocyte Ca2+ elevations and hemodynamic responses in mouse somatosensory cortex in vivo. *Proc Natl Acad Sci USA* 2013; **110**: E4678–E4687.
10 Nizar K, Uhlirova H, Tian P, Saisan PA, Cheng Q, Reznichenko L *et al.* In vivo stimulus-induced vasodilation occurs without IP3 receptor activation and may precede astrocytic calcium increase. *J Neurosci* 2013; **33**: 8411–8422.
11 Bonder DE, McCarthy KD. Astrocytic Gq-GPCR-linked IP3R-dependent Ca2+ signaling does not mediate neurovascular coupling in mouse visual cortex in vivo. *J Neurosci* 2014; **34**: 13139–13150.
12 Shigetomi E, Bushong EA, Haustein MD, Tong X, Jackson-Weaver O, Kracun S *et al.* Imaging calcium microdomains within entire astrocyte territories and endfeet with GCaMPs expressed using adeno-associated viruses. *J Gen Physiol* 2013; **141**: 633–647.
13 Otsu Y, Couchman K, Lyons DG, Collot M, Agarwal A, Mallet J-M *et al.* Calcium dynamics in astrocyte processes during neurovascular coupling. *Nat Neurosci* 2015; **18**: 210–218.
14 Schulz K, Sydekum E, Krueppel R, Engelbrecht CJ, Schlegel F, Schroter A *et al.* Simultaneous BOLD fMRI and fiber-optic calcium recording in rat neocortex. *Nat Methods* 2012; **9**: 597–602.
15 Chaigneau E, Wright AJ, Poland SP, Girkin JM, Silver RA. Impact of wavefront distortion and scattering on 2-photon microscopy in mammalian brain tissue. *Opt Express* 2011; **19**: 22755–22774.

Supplementary Information accompanies the paper on the Journal of Cerebral Blood Flow & Metabolism website (http://www.nature.com/jcbfm)